

# Proapoptotic Bcl-2 inhibitor as potential host directed therapy for pulmonary tuberculosis

Received: 22 August 2024

Accepted: 11 March 2025

Published online: 27 March 2025



Medha Singh<sup>1,2,3</sup>, Mona O. Sarhan<sup>1,2,3</sup>, Nerketa N. L. Damiba<sup>1,2</sup>, Alok K. Singh<sup>1,2,3,7</sup>, Andres Villabona-Rueda<sup>4</sup>, Oscar J. Nino-Meza<sup>1,2,3</sup>, Xueyi Chen<sup>1,2,3</sup>, Yuderleys Masias-Leon<sup>1,2,3</sup>, Carlos E. Ruiz-Gonzalez<sup>1,2,3</sup>, Alvaro A. Ordonez<sup>1,2,3</sup>, Franco R. D'Alessio<sup>4</sup>, Eric O. Aboagye<sup>5</sup>, Laurence S. Carroll<sup>6</sup> & Sanjay K. Jain<sup>1,2,3,6</sup> ✉

*Mycobacterium tuberculosis* establishes within host cells by inducing anti-apoptotic Bcl-2 family proteins, triggering necrosis, inflammation, and fibrosis. Here, we demonstrate that navitoclax, an orally bioavailable, small-molecule Bcl-2 inhibitor, significantly improves pulmonary tuberculosis (TB) treatments as a host-directed therapy. Addition of navitoclax to standard TB treatments at human equipotent dosing in mouse models of TB, inhibits Bcl-2 expression, leading to improved bacterial clearance, reduced tissue necrosis, fibrosis and decreased extrapulmonary bacterial dissemination. Using immunohistochemistry and flow cytometry, we show that navitoclax induces apoptosis in several immune cells, including CD68<sup>+</sup> and CD11b<sup>+</sup> cells. Finally, positron emission tomography (PET) in *live* animals using clinically translatable biomarkers for apoptosis (<sup>18</sup>F-ICMT-11) and fibrosis (<sup>18</sup>F-FAPI-74), demonstrates that navitoclax significantly increases apoptosis and reduces fibrosis in pulmonary tissues, which are confirmed in postmortem analysis. Our studies suggest that proapoptotic drugs such as navitoclax can potentially improve pulmonary TB treatments, reduce lung damage / fibrosis and may be protective against post-TB lung disease.

Despite being preventable and treatable, tuberculosis (TB) remains the second leading cause of mortality globally, with an estimated 1.25 million deaths and 10.8 million new cases due to TB, reported in 2023<sup>1</sup>. According to the World Health Organization (WHO), TB has become the leading cause of death globally from a single infectious agent again, surpassing coronavirus disease (COVID-19). Further, the burden of drug-resistant TB [DR-TB, including multidrug resistant (MDR)-TB

strains resistant to first-line TB drugs rifampin and isoniazid] continues to remain high with an estimated 400,000 new cases of rifampin resistant or MDR TB in 2023. The global community has established a goal to eradicate the TB epidemic by 2030, but achieving this objective necessitates urgent and innovative treatments.

During TB infection, early-stage apoptosis is host protective which results in immune clearance of *Mycobacterium tuberculosis*

<sup>1</sup>Center for Infection and Inflammation Imaging Research, Johns Hopkins University School of Medicine, Baltimore, MD, USA. <sup>2</sup>Center for Tuberculosis Research, Johns Hopkins University School of Medicine, Baltimore, MD, USA. <sup>3</sup>Department of Pediatrics, Johns Hopkins University School of Medicine, Baltimore, MD, USA. <sup>4</sup>Department of Medicine, Johns Hopkins University School of Medicine, Baltimore, MD, USA. <sup>5</sup>Comprehensive Cancer Imaging Centre, Department of Surgery & Cancer, Hammersmith Campus, Imperial College, London, UK. <sup>6</sup>Russell H. Morgan Department of Radiology and Radiological Science, Johns Hopkins University School of Medicine, Baltimore, MD, USA. <sup>7</sup>Present address: Amity Institute of Biotechnology, Amity University, Noida, Uttar Pradesh, India. ✉e-mail: [sjain5@jhmi.edu](mailto:sjain5@jhmi.edu)

infected cells, activating both innate and adaptive immune response<sup>2,3</sup>. At later stages, bacteria benefit from inhibiting apoptosis and promoting uncontrolled necrosis, which facilitates bacterial dissemination and persistence<sup>4–6</sup>. Necrosis increases TB-associated morbidity as it causes tissue destruction, promotes fibrosis, and thereby reduces the penetration of antibiotics to the regions where they are needed most. The necrotic granuloma also provides a breeding ground for *M. tuberculosis* replication and can transform into cavities, leading to an increased likelihood of developing antibiotic resistant bacteria, treatment failure, and transmission of bacteria to other individuals<sup>7</sup>. Necrotic tissues, often heal by fibrosis, leading to lung dysfunction long after treatment completion, which is increasingly being recognized as post-TB lung disease<sup>8</sup>. Conversely, apoptosis is host-protective by eliminating infected cells without triggering excessive inflammation<sup>9–12</sup>. Therefore, there has been recent interest in developing host-directed therapies (HDTs) that promote apoptosis<sup>13</sup>, and which could shorten the duration of TB treatments when given in combination with antibiotic regimens. Unlike antibiotics, HDTs modulate host cell responses to improve overall outcomes<sup>14,15</sup>, and currently, there are no clinically approved HDTs for pulmonary TB. Importantly, since HDTs target host (mammalian) cells without direct antibiotic effects, they are likely to work against drug-susceptible, as well as MDR *M. tuberculosis* strains<sup>16</sup>.

Here, we study navitoclax (ABT-263), an orally bioavailable, proapoptotic small molecule Bcl-2 inhibitor in clinical trials for cancer treatments, as an adjunctive HDT for pulmonary TB. Addition of navitoclax to the first-line, standard TB treatment (rifampin – R, isoniazid – H and pyrazinamide – Z, RHZ regimen) promotes pulmonary bacterial clearance and reduces lung damage in mouse models of TB, by inhibiting tissue Bcl-2 expression. Further, positron emission tomography (PET) in live animals with <sup>18</sup>F-(S)-1-(1-(2-fluoroethyl)-1H-[1,2,3]-triazol-4-yl)methyl)-5-(2(2,4-difluorophenoxymethyl)-pyrrolidine-1-sulfonyl) isatin (<sup>18</sup>F-ICMT-11), a clinically translatable imaging biomarker for apoptosis that targets activated caspase 3/7, demonstrated higher tissue apoptosis in navitoclax-treated animals, which was confirmed using postmortem analysis. Using immunohistochemistry and flow cytometry, we also demonstrate that navitoclax induces apoptosis in multiple cell types, including CD68<sup>+</sup> immune cells. Finally, addition of navitoclax to the standard TB treatment significantly reduces pulmonary fibrosis in live animals, as measured by <sup>18</sup>F-labeled fibroblast activation protein inhibitor (<sup>18</sup>F-FAPI-74) PET, a clinically translatable imaging biomarker for fibrosis (Figure S1), and confirmed on postmortem analysis. Extra-pulmonary bacterial dissemination was also decreased in animals receiving adjunctive navitoclax.

## Results

Wilson et al. performed a dose escalation study in cancer patients<sup>17</sup>, and a human dose of 315 mg/day demonstrated efficacy and was also well tolerated. The pharmacokinetic parameters [ $C_{\max}$  and area under the curve (AUC)] of this dose were equivalent to those noted in mice receiving 100 mg/kg/day<sup>18</sup> (Table S1), which has been used extensively in mice<sup>19,20</sup>, and therefore was chosen for our studies. To assess whether navitoclax could directly affect *M. tuberculosis*, we performed in vitro assays to measure the minimum inhibitory concentration (MIC). Navitoclax did not inhibit growth of *M. tuberculosis* at all concentrations tested (0.0078 to 32 µg/mL).

### Navitoclax reduces bacterial burden and lung pathology

TB treatments were initiated three weeks after an aerosol infection with *M. tuberculosis*. While treatment with navitoclax alone did not have any antimicrobial effects, when combined with the standard TB treatment (RHZ + navitoclax), there was a significant (albeit modest) reduction in the bacterial burden compared to the standard treatment alone (RHZ) ( $P < 0.01$ ) (Fig. 1a, S2a). The addition of navitoclax also improved lung pathology, with a significant decrease in the percentage

of lesion affected lung regions ( $P = 0.02$ ) (Fig. 1b, c). In another set of experiments, TB treatments were initiated six weeks after an aerosol infection with *M. tuberculosis*, when pulmonary fibrosis is well established in this model (chronic model)<sup>21</sup>. The overall trends in pulmonary bacterial reductions and lung pathology were similar (Figure S2b–e) with significantly lower bacterial burden (1.2 log<sub>10</sub> reduction) in mice receiving navitoclax in addition to the standard TB treatment at eight-weeks of treatment ( $P = 0.04$ ) (Fig. 1d). Additionally, the necrotic areas were quantified for lesions from each study arm and it was observed that the necrotic areas were substantially lower in mice treated with adjunctive navitoclax versus RHZ alone ( $P = 0.01$ ) (Fig. 1e, f). Furthermore, the addition of navitoclax to the standard TB treatment modestly reduced extrapulmonary dissemination to the spleen, and no bacterial dissemination to the brain was noted in mice receiving navitoclax in addition to the standard TB treatment (Figure S3a, b).

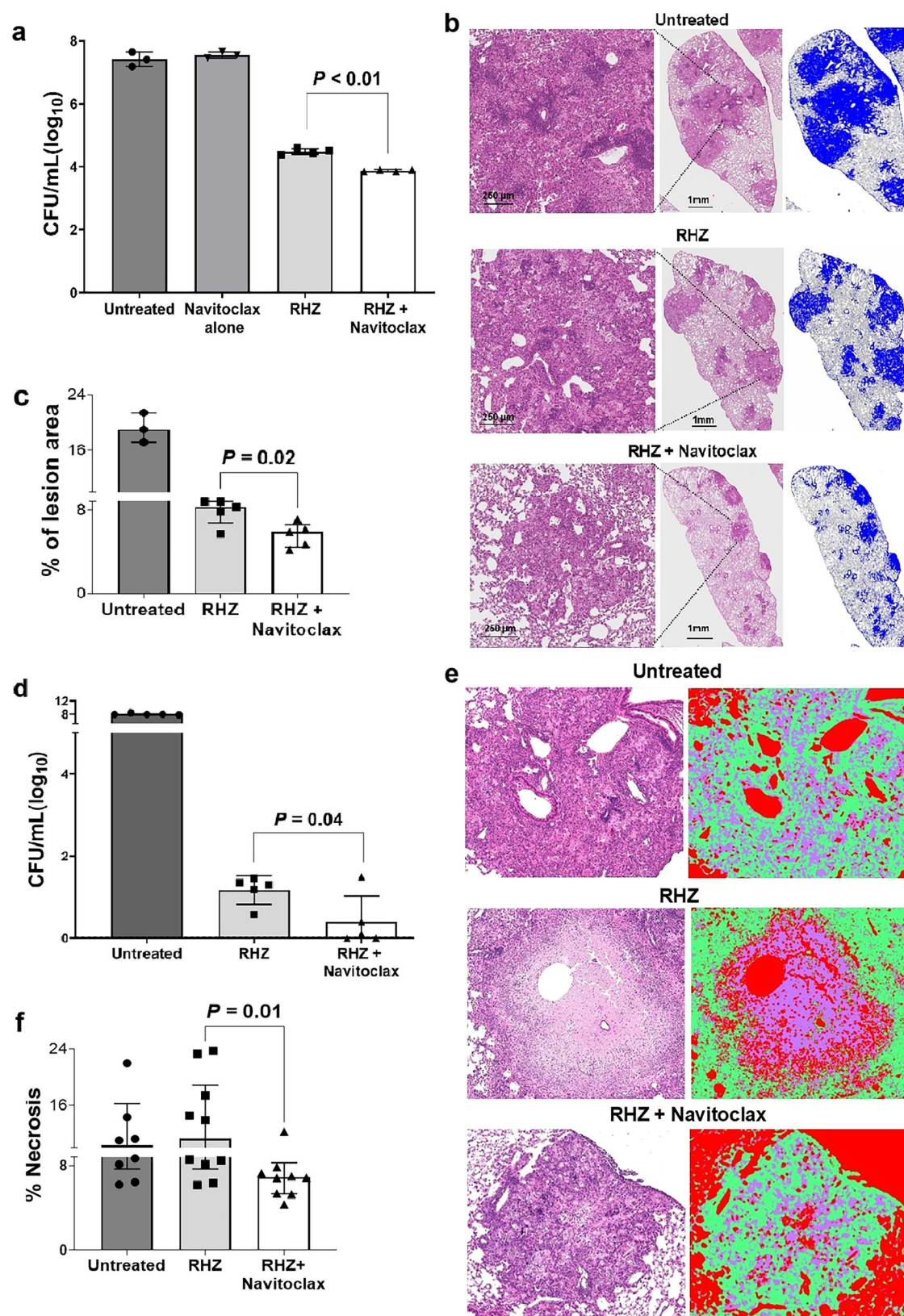
### Navitoclax induces lung tissue apoptosis by inhibiting Bcl-2

We have previously reported <sup>18</sup>F-ICMT-11 PET as a noninvasive approach to measure intralésional proapoptotic responses in situ in mice<sup>22</sup>. Dynamic PET was performed in live *M. tuberculosis*-infected mice within sealed biocontainment cells<sup>23,24</sup>, two weeks after initiation of TB treatments. Maximum intensity projection (MIP) and transverse <sup>18</sup>F-ICMT-11 PET/CT from representative *M. tuberculosis*-infected mice (Fig. 2a, S4) and quantification of pulmonary <sup>18</sup>F-ICMT-11 PET signal as percent injected dose/mL (%ID/mL) (Fig. 2b) are shown. <sup>18</sup>F-ICMT-11 PET area under the curve (AUC) was significantly higher in the lungs of animals treated with the standard TB treatment in addition to navitoclax versus those receiving the standard treatment alone ( $P = 0.01$ ) (Fig. 2c). Pulmonary <sup>18</sup>F-ICMT-11 PET activity was lowest in the untreated animals. To delineate the mechanistic basis of navitoclax effects, we assessed the tissue levels of anti-apoptotic proteins Bcl-2, and Bcl-xl which are inhibited by navitoclax, and Bim, Bid, Cytochrome C (Cyt C) (pro-apoptotic proteins) in whole lung lysates using western blots. Bcl-2 and Bcl-xl protein levels were significantly lower ( $P = 0.01$  and  $P = 0.04$ , respectively), and levels of Bim, Bid and Cyt C were significantly higher ( $P = 0.01$ ,  $P = 0.04$ , and  $P = 0.01$ , respectively) in animals receiving adjunctive navitoclax versus standard TB treatment alone (Fig. 2f–k). Similarly, apoptosis markers, Annexin V (Fig. 2d, S5), and caspase 3 (Fig. 2e) were significantly higher in mice receiving navitoclax plus standard TB treatment versus standard TB treatment alone ( $P \leq 0.01$ ).

### Effects of Navitoclax on immune cells in lung tissues

We investigated the cell types targeted by navitoclax in the lungs of *M. tuberculosis*-infected mice using high-dimensional flow cytometry (Figure S6). Isoniazid with or without navitoclax were initiated three weeks after a high dose aerosol infection. While the proportion of immune cells (CD45<sup>+</sup>) were similar in treatment groups with or without navitoclax (Fig. 3a–c), the addition of navitoclax led to a significant increase in apoptosis in several myeloid / macrophage lineage cells, two weeks after treatment initiation (Fig. 3d;  $P < 0.01$ ). Similar studies were performed in the chronic mice model where TB treatments (RHZ with and without navitoclax) were initiated six weeks after a low dose *M. tuberculosis* aerosol infection. Here, the addition of navitoclax demonstrated a similar trend for the proportion of immune cells and caspase 3 activity, four weeks after treatment initiation (Figure S7).

Next, we performed immunofluorescence in lung tissue from *M. tuberculosis*-infected mice undergoing standard TB treatments, with and without navitoclax, to identify the apoptotic effects of navitoclax in key immune cells. CD68 and CD11b are markers of myeloid / phagocytic cells critical in TB pathogenesis<sup>25–27</sup>, and consistent with the published studies, were localized within the TB lesions in all treatment arms. Importantly, the co-localization of cleaved caspase 3 (marker of apoptosis) was significantly higher in animals receiving adjunctive



navitoclax (versus standard TB treatment alone) with both CD68<sup>+</sup> ( $P = 0.03$ ) (Fig. 4a, b) and CD11b<sup>+</sup> ( $P = 0.01$ ) (Figure S8a, b) cells. The cumulative mean fluorescence intensity (MFI) for cleaved caspase 3, was significantly higher in animals receiving navitoclax plus standard TB treatment versus standard TB treatment alone (Fig. 4c, d, S8c, d).

Furthermore, we performed immunofluorescence assays using Auramine O to stain for *M. tuberculosis*. Image acquisition was performed for various channels (GFP for Auramine, Cy5 for cleaved caspase 3 and Cy3 for CD11b). Co-localization of the bacterial signal with the signal from caspase 3 was observed in the RHZ + navitoclax group (Figure S9).



**Fig. 1 | Navitoclax treatment in mouse model of pulmonary tuberculosis at human equipotent dosing.** *M. tuberculosis*-infected mice were randomly allocated to receive standard TB treatment (R, rifampin; H, isoniazid; Z, pyrazinamide) with or without navitoclax at human equipotent dosing via oral gavage. **a** TB treatments were initiated three weeks after a high dose aerosol infection. Bacterial burden [colony-forming unit (CFU) per mL ( $\log_{10}$ ) from whole lung] after three weeks of treatment ( $n = 3$  untreated mice, 3 navitoclax (alone) treated mice, 4 RHZ treated mice and 4 RHZ + navitoclax treated mice). When combined with the standard TB treatment (RHZ + navitoclax), there was a significant (albeit modest) reduction in the bacterial burden compared to the standard treatment alone (RHZ) ( $P < 0.01$ ). **b** Hematoxylin & Eosin (H&E) stained lung sections of mice demonstrating lung pathology. **c** The bar graph represents the percentage of affected lung tissue regions from H&E-stained lung tissue sections ( $n = 3$  tissue sections from untreated group and 5 tissue sections from RHZ and RHZ + Navitoclax treated group from 2 animals per group). The addition of navitoclax also improved lung pathology, with a significant decrease in the

percentage of lesion affected lung regions ( $P = 0.02$ ). **d** TB treatments were initiated six weeks after a low dose aerosol infection with *M. tuberculosis*, when fibrosis is well established (chronic model). Bacterial burden [colony-forming unit (CFU) per mL ( $\log_{10}$ ) from whole lung] after eight weeks of treatment ( $n = 5$  mice/group) are shown. Mice receiving navitoclax in addition to the standard TB treatment at eight-weeks of treatment had significantly lower bacterial burden (1.2  $\log_{10}$  reduction) ( $P = 0.04$ ). **e** Lung tissue H&E sections were used for quantification of necrosis using Trainable Weka Segmentation 3D plugin available in ImageJ Fiji ( $n = 5$  sections from each group). **f** Percent necrotic area was quantified for each lesion and shown as bar graph. Necrotic areas were substantially lower in mice treated with adjunctive navitoclax versus RHZ alone ( $P = 0.01$ ). For CFU, data are represented as mean  $\pm$  standard deviation and statistical comparisons were made using the student t-test. For affected and necrotic lung tissue regions, data are represented as median  $\pm$  interquartile range. Statistical comparisons were made using the Mann-Whitney U one-tailed test or the student two-tailed t-test (CFU data).

### Addition of Navitoclax to standard TB treatment reduces lung fibrosis

Fibroblast activation protein (FAP) is a type II transmembrane serine protease, highly expressed in fibrotic tissues at the remodelling interface in lung tissues<sup>28</sup>. We synthesized  $^{18}\text{F}$ -FAP-74 with a radiolabeling yield of  $15.4 \pm 0.1\%$  (non-decay corrected) and a radiochemical purity of  $97.5 \pm 0.1\%$ . The specific activity was  $69\text{--}101\text{ GBq}/\mu\text{mol}$  as determined by HPLC and corrected for the time at image acquisition (Figure S10). Dynamic  $^{18}\text{F}$ -FAP-74 PET was performed in *M. tuberculosis*-infected mice (chronic model) within sealed biocontainment cells<sup>23,24</sup>, demonstrating a significantly lower pulmonary PET signal quantified as  $\text{AUC}_{\text{lesion/blood}}$  in animals receiving adjunctive navitoclax versus standard TB treatment alone (Fig. 5a–c, S11). The anti-fibrotic effect of navitoclax was also confirmed using postmortem studies demonstrating significantly lower pulmonary fibrosis [Masson's trichrome staining ( $P < 0.01$ ) and soluble collagen levels ( $P = 0.02$ )] in animals receiving adjunctive navitoclax versus standard TB treatment alone (Fig. 6a–c). Analysis of several cytokines and chemokine markers were performed in plasma and from whole lung tissue homogenates from the chronic mouse model. Although TB treatments reduced proinflammatory cytokines and chemokine markers, there were no significant differences between the groups treated with RHZ with and without navitoclax (Figure S12). Finally, we assessed TGF- $\beta$ , which plays a pivotal role in fibrosis, using flow cytometry. TGF- $\beta$  levels in the lung tissues of navitoclax + RHZ (versus RHZ alone) treated animals were significantly lower in immune and non-immune cells (Fig. 3e;  $P = 0.03$ ).

### Co-administration of Rifampin does not affect Navitoclax levels in mice

Studies have shown that co-administration of navitoclax with rifampin moderately decreases (40%) navitoclax plasma levels in patients but does not change the  $C_{\text{max}}$ , half-life or its safety profile<sup>29</sup>. We measured navitoclax levels using mass spectrometry in *M. tuberculosis*-infected mice co-administrated with rifampin as part of the standard TB treatment. The median (interquartile range) for navitoclax plasma and lung levels were  $28.50$  ( $25.65\text{--}28.75$ )  $\mu\text{g}/\text{mL}$  and  $5.76$  ( $5.38\text{--}11.32$ )  $\mu\text{g}/\text{g}$ , respectively (Figure S13a, b), and consistent with published navitoclax levels achieved in mice without co-administration of TB treatments or rifampin<sup>18,30</sup>. We also measured plasma and lung tissue rifampin levels in mice receiving RHZ with and without navitoclax at steady state. No differences were noted in either lung or plasma levels in mice receiving RHZ with and without navitoclax ( $P > 0.33$ ) (Figure S13c, d).

### Navitoclax administration has no effect on platelet counts in mice

Given that reversible thrombocytopenia is the only major side effect of navitoclax in human studies<sup>17</sup>, we measured the platelets in blood

samples from *M. tuberculosis*-infected mice. The median platelet counts at three weeks into treatment in untreated mice, and those receiving standard TB treatments, with and without navitoclax were  $1.09 \times 10^6/\mu\text{L}$ ,  $1.05 \times 10^6/\mu\text{L}$  and  $0.99 \times 10^6/\mu\text{L}$ , respectively. There were no significant differences in the median platelet counts in mice receiving standard TB treatments with and without navitoclax ( $P = 0.43$ ) (Figure S14a–d). The platelet counts after eight weeks of treatment of navitoclax + RHZ (six weeks of navitoclax + RHZ and continued RHZ for the remaining two weeks) in the chronic mice model also demonstrated no difference from those receiving RHZ alone ( $P = 0.40$ ) (Figure S14e).

## Discussion

Current TB treatments comprise multidrug regimens, administered for 4–6 months, even for the treatment of uncomplicated pulmonary TB. Importantly, unlike other respiratory infections, many patients with TB have permanently damaged tissues with successful treatments only transitioning these TB patients from harboring a communicable infectious disease, to a syndrome of chronic pulmonary morbidity, commonly referred to as post-TB lung disease<sup>31,32</sup>. In one recent analysis of 6225 pulmonary TB patients, abnormal lung function was noted in 46.7%, persistent respiratory symptoms in 41.0%, and radiologic abnormalities in 64.6%<sup>32</sup>. Although the precise mechanisms underlying post-TB lung disease remain poorly characterized, it is primarily mediated by *M. tuberculosis*-induced host-tissue damage (necrosis) and subsequent fibrosis<sup>31</sup>. Currently, there are no approved treatments to prevent post-TB lung disease. Therefore, there is significant interest in developing HDTs that can not only improve TB treatments<sup>13,33,34</sup>, but also maintain lung function and protect against post-TB lung disease.

During the early stages of infection, *M. tuberculosis* evades apoptosis via induction of anti-apoptotic Bcl-2 family proteins, leading to necrosis, increased inflammation, and vascular disruptions, ultimately leading to fibrosis<sup>9,35</sup>. Therefore, the strategic targeting of apoptosis using HDTs presents a unique therapeutic approach to improve TB treatments. Among the orally bioavailable, proapoptotic small molecule Bcl-2 inhibitors, navitoclax and venetoclax are available for human use, with an excellent safety profile<sup>36</sup>. Venetoclax is a selective Bcl-2 inhibitor and approved by the U.S. FDA<sup>37</sup>, while navitoclax is in clinical trials. However, we choose navitoclax for these studies as it inhibits a wide spectrum of Bcl-2 family proteins (Bcl-2, Bcl-xl, Bcl-w, Mcl-1)<sup>38</sup>, targets multiple host cells, including myofibroblasts, exerting anti-fibrotic effect by blocking Bcl-xl, which can treat established fibrosis in several different organs<sup>20,36</sup>, and due to its safety profile. Co-administration of navitoclax with rifampin can moderately decrease navitoclax plasma levels<sup>29</sup>, but we demonstrate that this was not observed in our studies with *M. tuberculosis*-infected mice. Reversible thrombocytopenia is the only major side effect of navitoclax in human studies but daily dosing reduces thrombocytopenia risk

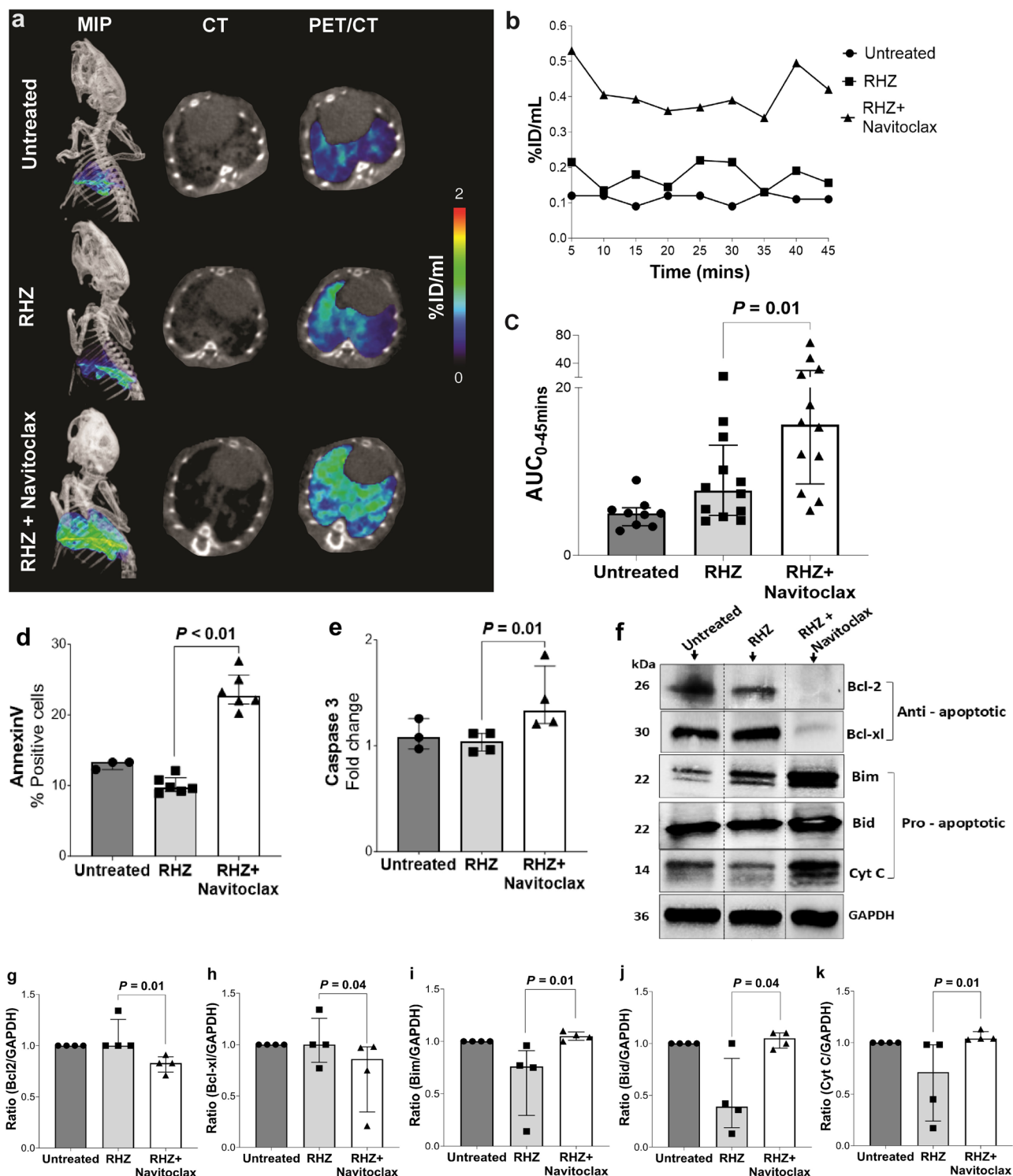


**Fig. 2 | Apoptosis quantification using imaging in live *M. tuberculosis*-infected mice and postmortem analysis.** TB treatments were initiated three weeks after a high dose aerosol infection. **a** Maximum intensity projection (MIP) and transverse  $^{18}\text{F}$ -ICMT-11 PET/CT from representative *M. tuberculosis*-infected mice from the different treatment arms, two weeks after initiation of TB treatments. Quantification of pulmonary  $^{18}\text{F}$ -ICMT-11 PET signal as percent injected dose/mL (%ID/mL) (panel **b**) and area under curve (AUC) (panel **c**) which was significantly higher in animals treated with the standard TB treatment in addition to navitoclax versus those receiving the standard TB treatment alone ( $P = 0.01$ ;  $n = 3$  untreated mice, 4 RHZ treated mice and 4 RHZ + navitoclax treated mice) are shown. **d** Flow cytometry of single-cell suspensions to analyse the percentage of Annexin V positive cells ( $n = 3$  animals per group; samples were acquired in duplicates for

some groups). **e** Lung tissue homogenate caspase 3 activity is shown ( $n = 4$  animals per group). Apoptosis markers, Annexin V ( $P < 0.01$ ) and caspase 3 ( $P = 0.01$ ) were significantly higher in mice receiving navitoclax plus standard TB treatment versus standard TB treatment alone. Levels of anti-apoptotic proteins Bcl2 and Bcl-xl (panels **f-h**), and pro-apoptotic proteins Bim, Bid, Cytochrome C (Cyt C) (panels **f, i-k**) from lung tissue homogenates using GAPDH as an internal control are shown ( $n = 4$  animals per group). Bcl-2 and Bcl-xl protein levels were significantly lower ( $P = 0.01$  and  $P = 0.04$ , respectively), and levels of Bim, Bid and Cyt C were significantly higher ( $P = 0.01$ ,  $P = 0.04$ , and  $P = 0.01$ , respectively) in animals receiving adjunctive navitoclax versus standard TB treatment alone. Data are represented as median  $\pm$  interquartile range. Statistical comparisons were made using the Mann-Whitney U one-tailed test.

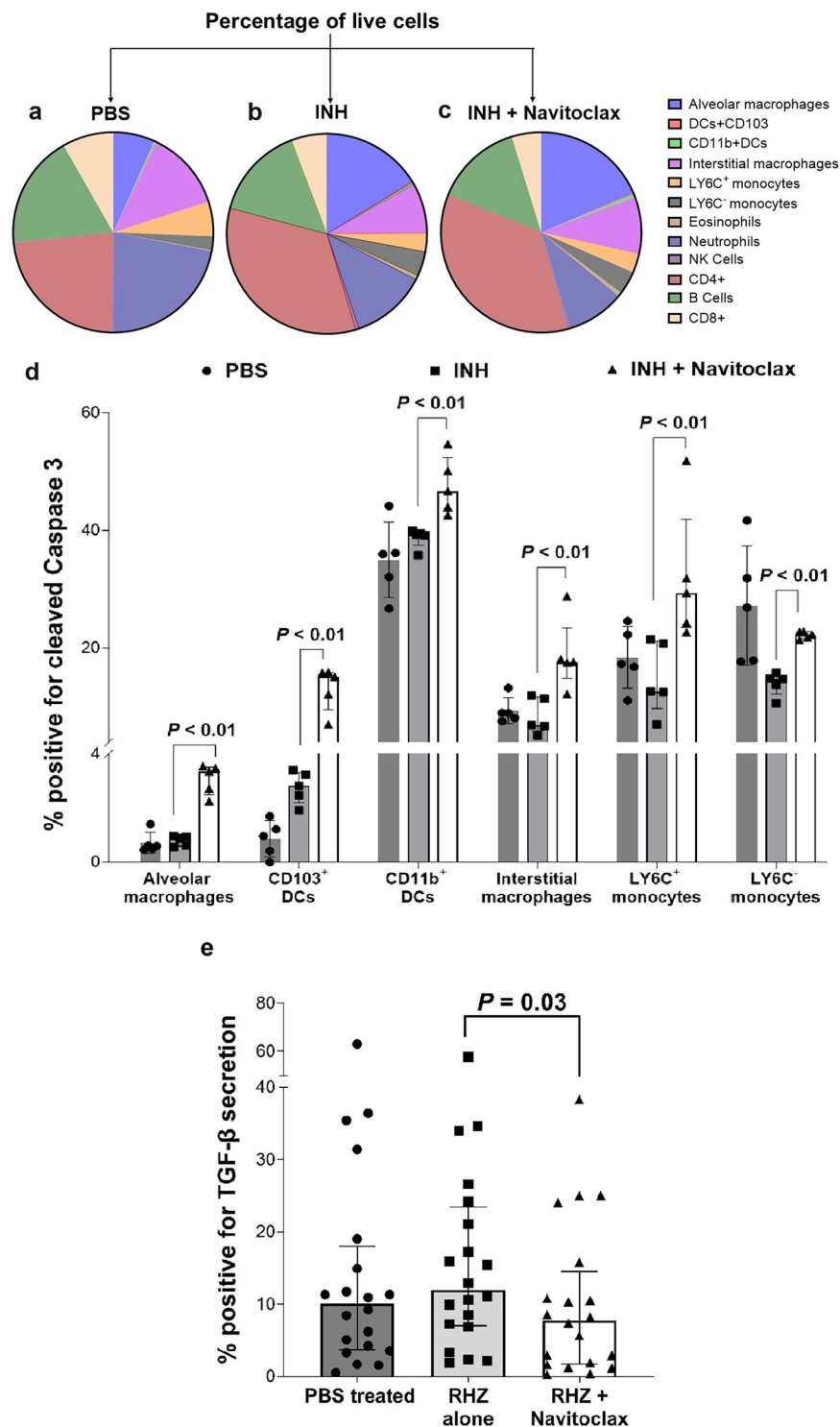


**Fig. 3 | High-dimensional flow cytometry in lung tissues.** Isoniazid with or without navitoclax were initiated three weeks after a high dose aerosol infection. Cell suspensions from lung tissues of *M. tuberculosis*-infected mice from the different treatment arms after exclusion of debris and doublets were analysed, two weeks after initiation of TB treatments. **a–c** Distribution of immune cells (CD45<sup>+</sup>) in the different treatment arms is shown. **d** Percentage of cells positive for intracellular expression of cleaved caspase 3 is shown. Five animals were used for each group. The addition of navitoclax led to a significant increase in apoptosis in several myeloid / macrophage lineage cells, two weeks after treatment initiation ( $P < 0.01$ ). **e** TB treatments (RHZ with or without navitoclax) were initiated six weeks after a

low dose aerosol infection with *M. tuberculosis*, when fibrosis is well established (chronic model). TGF- $\beta$  levels ( $n = 4$  mice/group) were assessed in CD45<sup>+</sup> immune cell populations (alveolar macrophage and interstitial macrophage) and CD45<sup>+</sup> non-immune cell populations (epithelial, endothelial and fibroblast) using flow cytometry. TGF- $\beta$  levels in the lung tissues of navitoclax + RHZ (versus RHZ alone) treated animals were significantly lower in immune and non-immune cells ( $P = 0.03$ ), four weeks after treatment initiation. Data are represented as median  $\pm$  interquartile range. Statistical comparisons were made using the Mann-Whitney one-tailed U test.



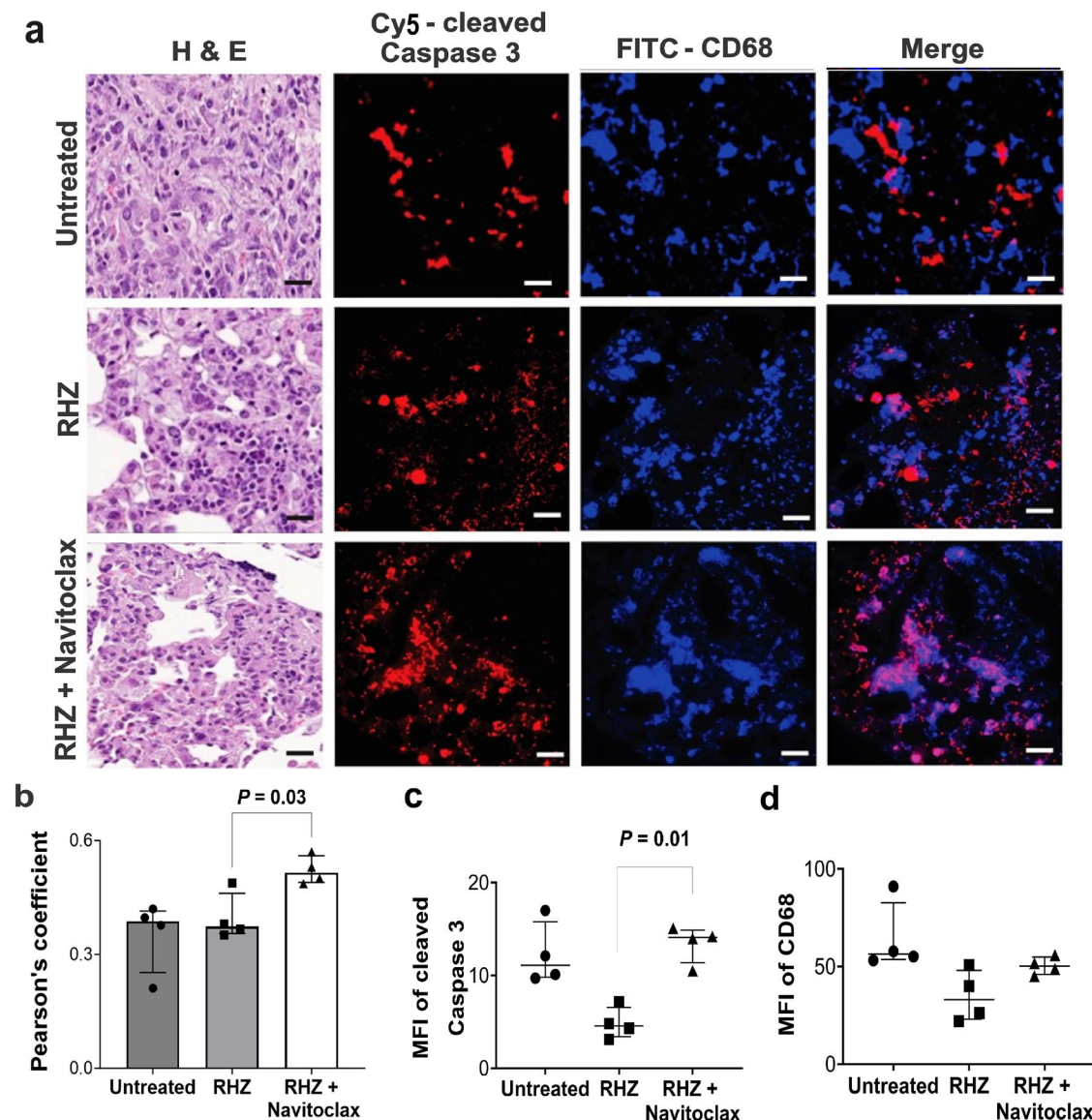


**Fig. 4 | Immunohistochemistry in lung tissues.** Fixed lung tissues from *M. tuberculosis*-infected mice from the different treatment arms, three weeks after initiation of TB treatments ( $n = 4$  sections/group; 2 sections per animal). TB treatments were initiated three weeks after a high dose aerosol infection. **a** H&E-stained images and immunostained panels - cleaved caspase 3, CD68 and merged are shown (40x magnification, scale bar 25  $\mu\text{m}$ ). **b** Pearson's coefficient to quantify colocalization of

cleaved caspase 3 and CD68 is shown. There is significantly higher colocalization of cleaved caspase 3 and CD68 in mice receiving navitoclax plus standard TB treatment versus those receiving standard treatment alone ( $P = 0.03$ ). Cumulative mean fluorescence intensity (MFI) for (c), cleaved caspase 3 (RHZ versus RHZ + navitoclax,  $P = 0.01$ ) and (d), CD68<sup>+</sup>. Data are represented as median  $\pm$  interquartile range. Statistical comparisons were made using the Mann-Whitney U one-tailed test.

to  $\sim 5\%$ <sup>17</sup>, which is less than with several commonly approved antibiotics<sup>39</sup>. Even though daily navitoclax dosing was used in our studies, we performed platelet counts in *M. tuberculosis*-infected mice which were consistent with the reported platelet counts for untreated adult mice (who did not receive TB treatments or rifampin)<sup>40–42</sup>, and were no differences between treatment groups with and without navitoclax, after 3 or 6-weeks of adjunctive navitoclax use with the standard TB treatments. Importantly, all clinical studies evaluating the risk of thrombocytopenia with navitoclax were performed in cancer patients who are already predisposed to thrombocytopenia due to their underlying disease and effects of prior or ongoing cancer treatments, which are likely not going to be present for TB patients.

We evaluated navitoclax at human equipotent dosing (315 mg/day) in combination with the first-line, standard TB treatment (RHZ), also administered at human equipotent dosing<sup>20</sup>. C3HeB/FeJ mice

were utilized as they develop human-like TB lung pathology<sup>3,7,21,43</sup> and accurately predict the effectiveness of TB regimens that have subsequently been translated to the clinic<sup>21,44,45</sup>. In vitro MIC testing confirmed that navitoclax did not inhibit the growth of *M. tuberculosis* and navitoclax also did not show any antimicrobial effect on its own in the animal studies. However, when combined with the standard TB treatment, navitoclax significantly (albeit modestly) decreased the pulmonary bacterial burden and improved lung pathology. Of note, while most HDTs decrease bacterial burden only modestly ( $\sim 1 \log_{10}$ , presumably targeting the  $\sim 1\text{--}2\%$  persister population)<sup>46,47</sup>, even this modest decrease in bacterial burden results in a substantial decrease ( $\sim 50\%$ ) in relapse<sup>46,47</sup>. Similar outcomes are anticipated with navitoclax, although definitive studies to assess relapse rates were not performed. *M. tuberculosis* can disseminate outside the lungs and cause extrapulmonary TB, including TB meningitis<sup>48,49</sup>. We observed that mice receiving adjunctive

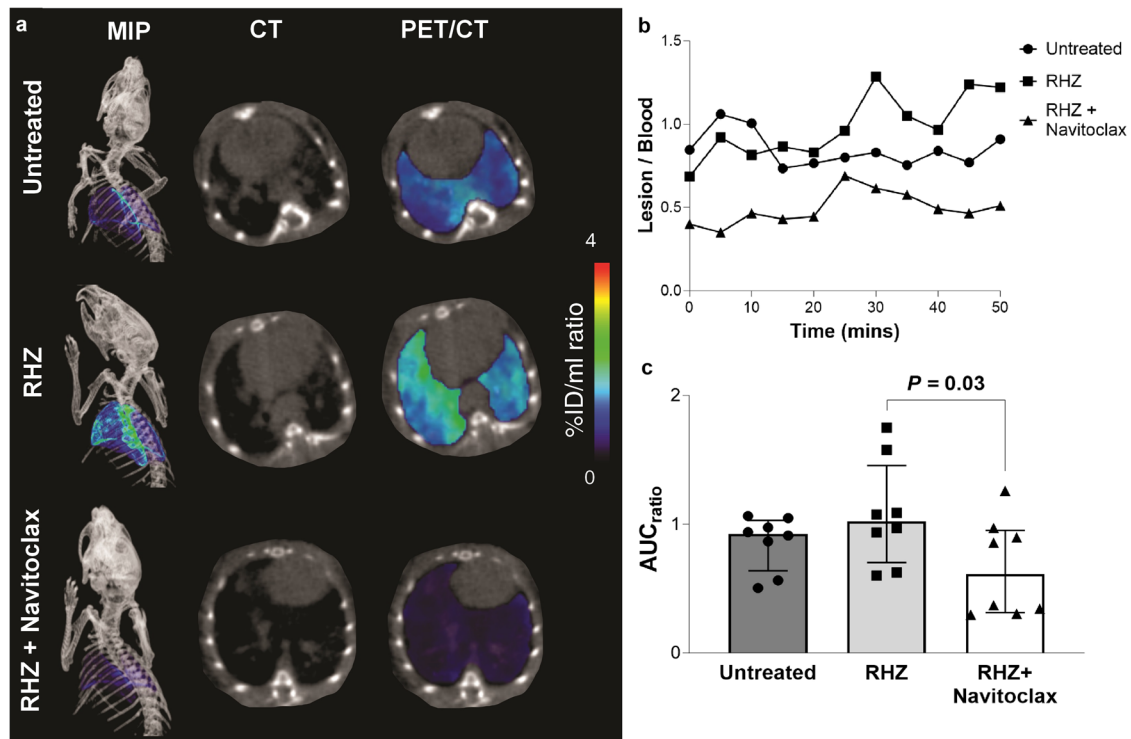


**Fig. 5 | Fibrosis imaging in live *M. tuberculosis*-infected mice.** TB treatments were initiated six weeks after a low dose aerosol infection with *M. tuberculosis*, when fibrosis is well established (chronic model). **a** Maximum intensity projection (MIP) and transverse  $^{18}\text{F}$ -FAPI-74 PET/CT from representative *M. tuberculosis*-infected mice from the different treatment arms, two weeks after initiation of TB treatments. Quantification of pulmonary  $^{18}\text{F}$ -FAPI-74 PET signal as lesion to blood ratio (panel **b**)

and heatmaps representing area under the curve (AUC<sub>lesion/blood</sub>) ratio (panel **c**) ( $n = 4$  mice/group) are shown. A significantly lower AUC<sub>lesion/blood</sub> was observed in animals receiving adjunctive navitoclax versus standard TB treatment alone ( $P = 0.03$ ). Data are represented as median  $\pm$  interquartile range. Statistical comparisons were made using the Mann-Whitney U one-tailed test.

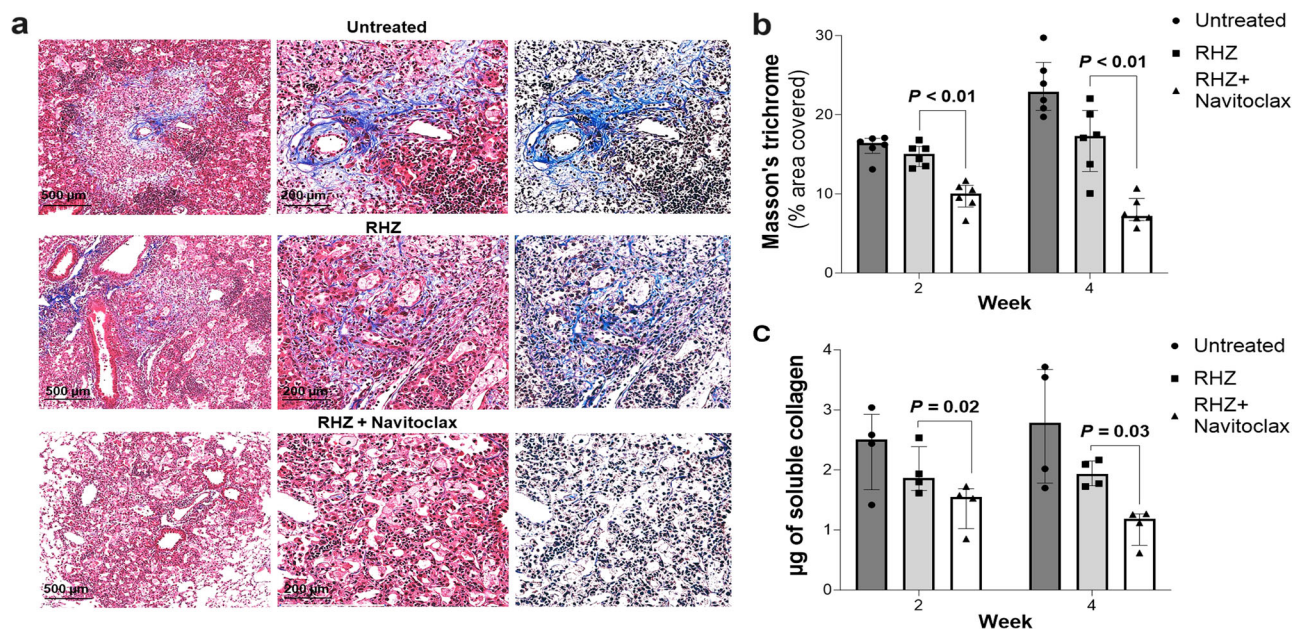


**Fig. 6 | Postmortem studies to quantify lung tissue fibrosis.** Fixed lung tissues from *M. tuberculosis*-infected mice (chronic model) from the different treatment arms were used two and four weeks after initiation of TB treatments ( $n = 6$  sections per group). Representative Masson's trichrome stained sections (panel **a**) and quantification (panel **b**) is shown. **c** Soluble collagen was quantified in whole lung

lysates ( $n = 4$  animals/group). A significantly lower pulmonary fibrosis [Masson's trichrome staining ( $P < 0.01$ ) and soluble collagen levels ( $P = 0.02$ )] was observed in animals receiving adjunctive navitoclax versus standard TB treatment alone. Data are represented as median  $\pm$  interquartile range. Statistical comparisons were made using the Mann-Whitney U one-tailed test.



navitoclax had modest decrease in the spleen bacterial burden and no bacterial dissemination to the brain. This is an interesting finding and is likely due to the proapoptotic effects of navitoclax, which can decrease extralésional bacterial dissemination. This highlights the potential role of navitoclax in preventing extrapulmonary dissemination and will be the subject of future investigation.

Since molecular and cellular alterations occur earlier than structural changes, molecular imaging is a powerful tool that has augmented early diagnosis, monitoring and investigation of various diseases<sup>50</sup>. Tomographic molecular imaging can evaluate disease processes deep within the body, noninvasively and relatively rapidly<sup>51–54</sup>. Although already critical in the management of patients with cancer, molecular imaging has similar potential for infectious diseases to provide molecular characterization of infected lesions, changes with progression or treatments, identification of patient-specific cellular and metabolic abnormalities and holistic three-dimensional visualization, which are less prone to sampling errors<sup>55</sup>. Here, we utilized clinically translatable molecular imaging tools to noninvasively assess navitoclax-induced pulmonary apoptosis (<sup>18</sup>F-ICMT-11) and TB-associated fibrosis (<sup>18</sup>F-FAPI-74) in live animals, which were confirmed using postmortem studies.

Since navitoclax is known to affect multiple cell types, we performed flow cytometry and immunofluorescence to define the immune cell profile as well as the key immune cell types targeted by navitoclax in our studies. Although the pulmonary immune cell profiles remained similar in mice receiving standard TB treatments, with or without navitoclax, administration of navitoclax-induced apoptosis in several myeloid / macrophage-lineage of immune cells. Additional studies utilizing immunofluorescence with CD11b, a pan myeloid marker and CD68, a marker for monocytes and macrophages<sup>27,56–58</sup> confirmed that navitoclax-induced apoptosis in these immune cells. Importantly, we provide mechanistic data that the effects of navitoclax are mediated by a decrease in anti-apoptotic proteins and increased expression of proapoptotic proteins. Finally, TGF- $\beta$ , which plays a pivotal role in fibrosis, was measured using flow cytometry in the lung tissues and demonstrated significantly lower levels in animals treated with navitoclax + RHZ versus RHZ alone, confirming its anti-fibrotic effects.

Our study has some limitations. We utilized a single age group and sex of mice, which may not fully capture sex-based variations in immune profiles, apoptosis, and fibrosis, across the age spectrum. Additionally, while imaging and postmortem studies provides valuable insights of pulmonary fibrosis, logistical and safety challenges in the BSL-3 environment prevented lung compliance and pulmonary function tests, such as forced expiratory volume. Future studies will address these parameters.

In summary, we demonstrate that navitoclax, an orally bioavailable, small-molecule Bcl-2 inhibitor, can improve pulmonary TB treatments by enhancing bacterial clearance and reducing tissue pathology. Addition of navitoclax to standard TB treatments at human equipotent dosing in mouse models of TB, decreases the expression of anti-apoptotic proteins, increases expression of proapoptotic proteins, leading to improved bacterial clearance, reduced tissue damage / fibrosis and decreased extrapulmonary bacterial dissemination. Finally, live imaging with clinically translatable biomarkers for apoptosis and fibrosis demonstrates that navitoclax significantly increases apoptosis and reduces fibrosis in pulmonary tissues. In the future, we anticipate that these imaging approaches could be used to non-invasively characterize post-TB lung disease as well as evaluate HDTs in early clinical trials.

## Methods

### Ethics statement

All protocols were approved by the Johns Hopkins University Biosafety, Radiation Safety, and Animal Care and Use Committees (MO19M382).

### In vitro minimum inhibitory concentration (MIC) testing for Navitoclax

*M. tuberculosis* frozen bacterial stock was cultured in Middlebrook 7H9 broth supplemented with 10% (vol/vol) Middlebrook OADC supplement, 0.1% (vol/vol) glycerol, and 0.05% (vol/vol) Tween 80 to an OD<sub>600</sub> of 1. The bacterial suspensions were then washed three times in PBS. Cultures were then diluted to an OD<sub>600</sub> of 0.1. Navitoclax (MedChem express) was tested at 13 different concentrations (32–0.0078  $\mu$ g/mL) performed by broth microdilution and plate-based REMA (resazurin microtiter assay) (Sigma-Aldrich) method in 7H9 broth using a standard reading time of 14 days. As a control, bedaquiline was included in the plate-based REMA method and showed a MIC of 0.05  $\mu$ g/mL, which is consistent with reported studies<sup>59</sup>.

### Animal infection and treatments

Six-to-seven week-old female C3HeB/FeJ (Jackson Laboratory) mice were aerosol infected with frozen titrated bacterial stocks of *M. tuberculosis* H37Rv using the Middlebrook Inhalation Exposure System (Glas-Col)<sup>43</sup>. Animals were housed within the ABSL-3 facility with a 12 h light cycle, a temperature range of 64–79 °F (18–26 °C), and a humidity range of 30–70% and *ad libitum* access to food and water. Five mice were sacrificed using isoflurane (Henry Schein) overdose one day of infection to assess implantation and just prior to treatment initiation to assess the bacterial burden. At the start of treatments, animals were randomly allocated to receive standard TB treatment with or without navitoclax. Untreated animals served as controls, and in some studies, navitoclax was administered alone. All drugs were administered via oral gavage, five days per week, at human equipotent dosing: rifampin (10 mg/kg/day), isoniazid (10 mg/kg/day), pyrazinamide (150 mg/kg/day) and navitoclax (100 mg/kg/day; MedChemExpress)<sup>20</sup>. After animal euthanasia, whole organs were removed aseptically, homogenized in phosphate-buffered saline (PBS), and plated by serial dilution onto Middlebrook 7H11 agar plates, which were incubated at 37 °C for three weeks before CFU were counted.

### Imaging

Imaging was performed in live *M. tuberculosis*-infected mice within sealed biocontainment cells<sup>23,24</sup> using the nanoScan PET/CT (Mediso). <sup>18</sup>F-ICMT-11 was synthesized using an acetal protected tosylate precursor (Figure S10a)<sup>22,60</sup>, while <sup>18</sup>F-FAPI-74 was synthesized as outlined (Figure S10b)<sup>61,62</sup>. For anatomical co-registration, a CT was acquired following the PET. Four hours after oral administration of navitoclax, mice received  $3.09 \pm 0.88$  MBq of <sup>18</sup>F-ICMT-11 via the tail vein and dynamic PET (45 min) was performed 15 min post-tracer injection. Dynamic PET (60 min) was performed immediately after an intravenous injection of  $3.93 \pm 0.86$  MBq of <sup>18</sup>F-FAPI-74 via tail vein. Volumes of interest (VOIs) were drawn manually using the CT as reference using VivoQuant 4.0 (Invivo) and the PET signal quantified from the registered images<sup>51</sup>. Heatmap overlays were created using AMIRA 5.2.1 (Visage Imaging, Inc.) and AMIDE 1.0.6 (Andreas Loening). <sup>18</sup>F-ICMT-11 PET was represented as percent (%) injected dose (ID) per volume of tissue (mL)<sup>22</sup>. <sup>18</sup>F-FAPI-74 PET was represented as lesion to blood AUC ratio<sup>61,62</sup>, with blood signal obtained by placing a VOI in the left ventricle of the heart.

### Histopathology and Immunofluorescence

Lungs were harvested after systemic perfusion with PBS, fixed in 4% paraformaldehyde. The lung lesions were identified on H&E stains and quantified using FIJI ImageJ (NIH). The quantification of necrosis was assessed using Trainable Weka Segmentation 3D plugin available in ImageJ FIJI (NIH). Briefly, lesions from low power lung sections were used to generate classifiers for categorizing unaffected areas, lesion area and necrotic areas within the lung. Percent necrotic area was quantified for each lung section. Masson's trichrome stains were used to assess fibrosis and quantified using FIJI ImageJ (NIH) using Colour

Deconvolution2 plugin enabled with Masson's trichrome vector for analysis.

Immunostaining was performed at the Johns Hopkins Oncology Tissue Services Core on formalin-fixed, paraffin-embedded sections using a Ventana Discovery Ultra autostainer (Roche Diagnostics). Primary antibody (anti-CD68, 1:300 dilution, ab125212, Abcam; anti-CD11b, 1:9000 dilution, ab133357, Abcam; anti-cleaved caspase 3, 1:1000 dilution, 9661S, Cell Signalling Technology) was applied at 36 °C for 40 min. Primary antibodies were detected using an anti-rabbit HQ detection system (7017936001 and 7017812001, Roche Diagnostics) followed by OPAL 520 (FP1487001KT, Akoya Biosciences) diluted 1:150 in 1X Plus Amplification Diluent (FP1498, Akoya Biosciences). Image acquisition was performed using the Leica DM6B system (Leica).

To overlap apoptosis with bacterial growth, we performed additional immunofluorescence assay using Auramine O to stain *M. tuberculosis* on these histological tissue sections belonging to RHZ and RHZ + navitoclax treated group of animals. Lesions were visualized under 100x magnification under Leica DM6B microscope and image acquisition was done for various channels (GFP for Auramine, Cy5 for cleaved caspase 3 and Cy3 for CD11b).

### Plasma and lung homogenate assays

Plasma and lung tissue homogenates were extracted and navitoclax levels were measured from three animals/group using mass spectrometry (Johns Hopkins Oncology core)<sup>63</sup> four hours after receiving 100 mg/kg of oral navitoclax. Briefly, navitoclax-d8 (MedChemExpress) was used as a standard. The LC system was a Shimadzu Nexera X<sup>2</sup> UHPLC system (Columbia, MD) with the autosampler operating at 5 °C. Analyte separation was achieved using a Waters Acquity UPLC BEH C<sub>18</sub> column (50 × 2.1 mm, 1.7 µm, Milford, MA, USA) at 40 °C. Sample elution was done using a mixture of acetonitrile: water: formic acid (70:30:0.1 v/v) at 0.15 mL/min flow rate and isocratic elution. An AB SCIEX 4500 triple quadrupole mass spectrometer was operated in positive electrospray ionization utilizing multiple reaction monitoring (MRM) mode. The LC and the mass spectrometer were controlled by the Analyst software (version 1.6.2 and later). Plasma and lung tissue rifampin levels were measured using validated ultra-high-performance liquid chromatography (UPLC) and tandem mass spectrometry (LC-MS/MS) at the Infectious Diseases Pharmacokinetics Laboratory of the University of Florida (standard curves from 50.00 to 0.05 µg/mL)<sup>51,64</sup>. The assays measured both the free and protein-bound rifampin and multiple lesions were obtained per lung.

For studies used to determine platelet levels, fresh blood was collected in EDTA tubes. Blood smears were fixed in cold methanol followed by Wright-Giemsa staining (ab245888) and counted at 100x magnification. The platelet count was obtained using methods described previously<sup>40–42</sup>. Briefly, each slide was scanned at 100x magnification and total number of platelets were counted manually for each field of view. Platelets/µL was calculated by multiplying the number of platelets counted with 20000.

Soluble collagen was quantified in whole lung homogenates using fluorometric Soluble Collagen Quantification Assay Kit (Sigma, CS0006). Fluorescent intensity was measured at 465 nm (excitation 375 nm) and µg of soluble collagen was calculated using a standard curve.

Western blot analysis was performed using a standardized protocol using primary antibodies specific to GAPDH (MA5-15738, Thermo Fisher, dilution 1:1,000), Bid (ab272880, Abcam, dilution 1:1,000), Bcl-2 (ab182858, Abcam, dilution 1:1,000), Bim (2819S, Cell Signaling Technology, dilution 1:1000), Bcl-xl (2762S, Cell Signaling Technology, dilution 1:1000), Cytochrome C (4272 T, Cell Signaling Technology, dilution 1:1000) and a goat, anti-Rabbit (ab97051, dilution 1:5,000) secondary antibody. The protein bands were visualized on the membranes using chemiluminescent substrates (Supersignal

West Pico maximum sensitivity substrate, cat. no. 34580) and analysed using Fiji ImageJ (NIH).

Caspase 3 activity was quantified four hours after oral administration of navitoclax in mice using the caspase 3 assay kit (Abcam, ab39383) according to the manufacturer's protocol<sup>22</sup>. Briefly, lung tissues were homogenized and then lysed in the lysis buffer followed by incubation for 2 h in reaction buffer and DEVD-AFC substrate. Fluorometric analysis was performed with a 400 nm-excitation and 505 nm-emission filter using microplate reader (FLUOstar OPTIMA FL microplate reader, BMG Labtech). Caspase 3 activity was quantified as fold-increase relative to uninfected animals<sup>65</sup>. Annexin V (Thermo Fisher Scientific, A13199) assays were performed using single-cell lung tissue suspensions analysed using the LSRII flow cytometer (BD) and Flowjo v10.8 software (BD).

Cytokines and chemokine markers were assessed in plasma and from whole lung tissue homogenates at 4 weeks into TB treatments from the chronic mouse model where TB treatments were initiated six weeks after a low dose aerosol infection with *M. tuberculosis*. Assay was performed using Meso Scale Discovery kit (U-PLEX Custom Biomarker Group 1 (ms) Assays, K15069M-1), by the Johns Hopkins University Institute for Clinical & Translational Research (ICTR) Research Laboratory Core.

### Flow cytometry

Three weeks after an aerosol challenge with *M. tuberculosis* mice were randomly allocated to receive PBS, or isoniazid with or without navitoclax. All drugs were administered via oral gavage, five days per week, at human equipotent dosing: isoniazid (10 mg/kg/day), and navitoclax (100 mg/kg/day; MedChemExpress). Two weeks after treatment initiation, mice were sacrificed with isoflurane overdose, lungs were harvested and single-cell suspensions were prepared. Surface staining was performed by incubating samples with a master mix of surface antibodies (Table S2). For caspase 3 staining, primary and secondary antibodies were added sequentially during permeabilization. Flow cytometry was conducted using the FACS ARIA II. The gating strategy adhered to guidelines from the American Thoracic Society (Figure S6a). Initial steps involved removing debris, excluding doublets and dead cells, identifying immune cells (CD45<sup>+</sup>) (Brilliant Violet 750™ anti-mouse CD45 Antibody, BioLegend, Clone 30-F11), and excluding lymphoid cells (CD3<sup>+</sup> (PE/Cyanine5 anti-mouse CD3 Antibody, BioLegend, Clone 17A2), CD19<sup>+</sup>, PE anti-mouse CD19 Antibody, BioLegend, Clone 1D3/CD19)). Myeloid cells were further delineated based on CD11b (PE/Dazzle™ 594 anti-mouse/human CD11b Antibody, BioLegend, Clone M1/70) and CD11c (CD11c Hamster anti-Mouse, APC-R700, BD Horizon™, Clone: N418) positivity.

Similar protocol was followed for flow cytometry at four weeks into TB treatments using lung single cell suspensions from the chronic mice model where TB treatments were initiated six weeks after an aerosol infection with *M. tuberculosis*. TGF-β (Brilliant Violet 421™ anti-mouse LAP (TGF-β1) Antibody, BioLegend, Clone TW7 16B4) levels were assessed in CD45<sup>+</sup> (immune cells, alveolar and interstitial macrophages) and CD45<sup>−</sup> (non-immune cells, epithelia, endothelia and fibroblasts) using flow cytometry (Table S2, Figure S6b).

### Statistical analysis

Data were analysed using Prism 10 Version 10.1.1 (GraphPad). Bacterial burden (CFU) are represented on a logarithmic scale (base 10) as mean ± SD and comparisons were made using a student t-test. All other data are represented as median ± IQR and comparisons were made using a Mann-Whitney U test. *P* values ≤ 0.05 were considered statistically significant.

### Reporting summary

Further information on research design is available in the Nature Portfolio Reporting Summary linked to this article.

## Data availability

All data are available in the main text or the supplementary materials. Source data are provided with this paper.

## References

1. WHO. Global Tuberculosis Report (2024).
2. Malik, Z. A., Iyer, S. S. & Kusner, D. J. Mycobacterium tuberculosis phagosomes exhibit altered calmodulin-dependent signal transduction: contribution to inhibition of phagosome-lysosome fusion and intracellular survival in human macrophages. *J. Immunol.* **166**, 3392–3401 (2001).
3. Pan, H. et al. Ipr1 gene mediates innate immunity to tuberculosis. *Nature* **434**, 767–772 (2005).
4. Aguiló, N., Marinova, D. & Martin, C. J. P. ESX-1-induced apoptosis is involved in cell-to-cell spread of *Mycobacterium tuberculosis*. *Cell Microbiol.* **15**, 1994–2005 (2013).
5. Behar, S. M. et al. Apoptosis is an innate defense function of macrophages against. *Mucosal Immunol.* **4**, 279–287 (2011).
6. Zhang, J., Jiang, R., Takayama, H. & Tanaka, Y. Survival of virulent *Mycobacterium tuberculosis* involves preventing apoptosis induced by Bcl-2 upregulation and release resulting from necrosis in J774 macrophages. *Microbiol. Immunol.* **49**, 845–852 (2005).
7. Urbanowski, M. E., Ordonez, A. A., Ruiz-Bedoya, C. A., Jain, S. K. & Bishai, W. R. Cavitory tuberculosis: the gateway of disease transmission. *Lancet Infect. Dis.* **20**, e117–e128 (2020).
8. DiFazio, R. M. et al. Active transforming growth factor- $\beta$  is associated with phenotypic changes in granulomas after drug treatment in pulmonary tuberculosis. *Fibrogenes. tissue repair* **9**, 1–11 (2016).
9. Sly, L. M., Hingley-Wilson, S. M., Reiner, N. E. & McMaster, W. R. Survival of *Mycobacterium tuberculosis* in host macrophages involves resistance to apoptosis dependent upon induction of antiapoptotic Bcl-2 family member Mcl-1. *J. Immunol.* **170**, 430–437 (2003).
10. Wang, Q. M., Liu, S. P., Tang, Y., Liu, Q. H. & Yao, Y. J. MPT64 Protein from *Mycobacterium tuberculosis* Inhibits Apoptosis of Macrophages through NF- $\kappa$ B-miRNA21-Bcl-2 Pathway. *Plos One* **9**, e100949 (2014).
11. Zhao, X. et al. Bcl-x(L) mediates RIPK3-dependent necrosis in *M. tuberculosis*-infected macrophages. *Mucosal Immunol.* **10**, 1553–1568 (2017).
12. Gan, H. et al. Mycobacterium tuberculosis blocks crosslinking of annexin-1 and apoptotic envelope formation on infected macrophages to maintain virulence. *Nat. Immunol.* **9**, 1189–1197 (2008).
13. Arnett, E. et al. Combination of MCL-1 and BCL-2 inhibitors is a promising approach for a host-directed therapy for tuberculosis. *Biomedicine Pharmacother.* **168**, 115738 (2023).
14. Wilkinson, R. J. Host-directed therapies against tuberculosis. *Lancet Respir. Med* **2**, 85–87 (2014).
15. Zumla, A. et al. Host-directed therapies for infectious diseases: current status, recent progress, and future prospects. *Lancet Infect. Dis.* **16**, e47–e63 (2016).
16. Kaufmann, S. H. E., Dorhoi, A., Hotchkiss, R. S. & Bartenschlager, R. Host-directed therapies for bacterial and viral infections. *Nat. Rev. Drug Discov.* **17**, 35–56 (2018).
17. Wilson, W. H. et al. Navitoclax, a targeted high-affinity inhibitor of BCL-2, in lymphoid malignancies: a phase 1 dose-escalation study of safety, pharmacokinetics, pharmacodynamics, and antitumour activity. *Lancet Oncol.* **11**, 1149–1159 (2010).
18. Tse, C. et al. ABT-263: a potent and orally bioavailable Bcl-2 family inhibitor. *Cancer Res* **68**, 3421–3428 (2008).
19. Chen, J. et al. The Bcl-2/Bcl-X(L)/Bcl-w inhibitor, navitoclax, enhances the activity of chemotherapeutic agents in vitro and in vivo. *Mol. Cancer Ther.* **10**, 2340–2349 (2011).
20. Lagares, D. et al. Targeted apoptosis of myofibroblasts with the BH3 mimetic ABT-263 reverses established fibrosis. *Sci. Transl. Med* **9**, eaal3765 (2017).
21. Harper, J. et al. Mouse model of necrotic tuberculosis granulomas develops hypoxic lesions. *J. Infect. Dis.* **205**, 595–602 (2012).
22. Ordonez, A. A. et al. Caspase-Based PET for Evaluating Pro-Apoptotic Treatments in a Tuberculosis Mouse Model. *Mol. Imaging Biol.* **22**, 1489–1494 (2020).
23. Davis, S. L. et al. Noninvasive pulmonary [18F]-2-fluoro-deoxy-D-glucose positron emission tomography correlates with bactericidal activity of tuberculosis drug treatment. *Antimicrob. Agents Chemother.* **53**, 4879–4884 (2009).
24. Weinstein, E. A. et al. Noninvasive determination of 2-[18F]-fluoroisonicotinic acid hydrazide pharmacokinetics by positron emission tomography in *Mycobacterium tuberculosis*-infected mice. *Antimicrob. Agents Chemother.* **56**, 6284–6290 (2012).
25. Carow, B. et al. Spatial and temporal localization of immune transcripts defines hallmarks and diversity in the tuberculosis granuloma. *Nat. Commun.* **10**, 1823 (2019).
26. McCaffrey, E. F. et al. The immunoregulatory landscape of human tuberculosis granulomas. *Nat. Immunol.* **23**, 318–329 (2022).
27. Abengozar-Muela, M. et al. Diverse immune environments in human lung tuberculosis granulomas assessed by quantitative multiplexed immunofluorescence. *Mod. Pathol.* **33**, 2507–2519 (2020).
28. Acharya, P. S., Zukas, A., Chandan, V., Katzenstein, A. L. & Pure, E. Fibroblast activation protein: a serine protease expressed at the remodeling interface in idiopathic pulmonary fibrosis. *Hum. Pathol.* **37**, 352–360 (2006).
29. Yang, J. et al. Effect of rifampin on the pharmacokinetics, safety and tolerability of navitoclax (ABT-263), a dual inhibitor of Bcl-2 and Bcl-XL, in patients with cancer. *J. Clin. Pharm. Ther.* **39**, 680–684 (2014).
30. Bell, H. L. et al. Combination p53 activation and BCL-x(L)/BCL-2 inhibition as a therapeutic strategy in high-risk and relapsed acute lymphoblastic leukemia. *Leukemia* **38**, 1223–1235 (2024).
31. Allwood, B. W. et al. Post-tuberculosis lung health: perspectives from the First International Symposium. *Int J. Tuberc. Lung Dis.* **24**, 820–828 (2020).
32. Maleche-Obimbo, E. et al. Magnitude and factors associated with post-tuberculosis lung disease in low- and middle-income countries: A systematic review and meta-analysis. *PLOS Glob. Public Health* **2**, e0000805 (2022).
33. Arnett, E. & Schlesinger, L. S. Live and let die: TB control by enhancing apoptosis. *Immunity* **54**, 1625–1627 (2021).
34. Cubillos-Angulo, J. M. et al. Host-directed therapies in pulmonary tuberculosis: Updates on anti-inflammatory drugs. *Front Med (Lausanne)* **9**, 970408 (2022).
35. Stutz, M. D. et al. Macrophage and neutrophil death programs differentially confer resistance to tuberculosis. *Immunity* **54**, 1758–1771 e1757 (2021).
36. Mohamad Anuar, N. N., Nor Hisam, N. S., Liew, S. L. & Ugusman, A. Clinical review: navitoclax as a pro-apoptotic and anti-fibrotic agent. *Front. Pharmacol.* **11**, 564108 (2020).
37. Roberts, A. W. et al. Targeting BCL2 with venetoclax in relapsed chronic lymphocytic leukemia. *N. Engl. J. Med.* **374**, 311–322 (2016).
38. Roberts, A. W. et al. Substantial susceptibility of chronic lymphocytic leukemia to BCL2 inhibition: results of a phase I study of navitoclax in patients with relapsed or refractory disease. *J. Clin. Oncol.* **30**, 488–496 (2012).
39. Savage-Elliott, I., Wu, V. J. & Sanchez, F. L. Drug-Induced Thrombocytopenia Secondary to Commonly Used Antibiotics in Total Joint Arthroplasty. *Arthroplast Today* **6**, 137–140 (2020).



40. Aurbach, K., Spindler, M., Haining, E. J., Bender, M. & Pleines, I. Blood collection, platelet isolation and measurement of platelet count and size in mice—a practical guide. *Platelets* **30**, 698–707 (2019).
41. Peters, L. L. et al. Large-scale, high-throughput screening for coagulation and hematologic phenotypes in mice. *Physiol. Genomics* **11**, 185–193 (2002).
42. Jirouskova, M., Shet, A. S. & Johnson, G. J. A guide to murine platelet structure, function, assays, and genetic alterations. *J. Thromb. Haemost.* **5**, 661–669 (2007).
43. Ordóñez, A. A. et al. Mouse model of pulmonary cavitary tuberculosis and expression of matrix metalloproteinase-9. *Dis. Model Mech.* **9**, 779–788 (2016).
44. Xu, J. et al. Contribution of pretomanid to novel regimens containing bedaquiline with either linezolid or moxifloxacin and pyrazinamide in murine models of tuberculosis. *Antimicrob. Agents Chemother.* **63**, <https://doi.org/10.1128/aac.00021-00019> (2019).
45. Tasneen, R. et al. Sterilizing Activity of Novel TMC207-and PA-824-Containing Regimens in a Murine Model of Tuberculosis. *Antimicrobial Agents Chemother.* **55**, 5485–5492 (2011).
46. Ordóñez, A. A. et al. Adjunct antibody administration with standard treatment reduces relapse rates in a murine tuberculosis model of necrotic granulomas. *Plos One* **13**, e0197474 (2018).
47. Skerry, C., Harper, J., Klunk, M., Bishai, W. R. & Jain, S. K. Adjunctive TNF inhibition with standard treatment enhances bacterial clearance in a murine model of necrotic TB granulomas. *Plos One* **7**, e39680 (2012).
48. Jain, S. K. et al. Tuberculous meningitis: a roadmap for advancing basic and translational research. *Nat. Immunol.* **19**, 521–525 (2018).
49. Be, N. A., Kim, K. S., Bishai, W. R. & Jain, S. K. Pathogenesis of central nervous system tuberculosis. *Curr. Mol. Med.* **9**, 94–99 (2009).
50. Rowe, S. P. & Pomper, M. G. Molecular imaging in oncology: Current impact and future directions. *CA Cancer J. Clin.* **72**, 333–352 (2022).
51. Ordóñez, A. A. et al. Dynamic imaging in patients with tuberculosis reveals heterogeneous drug exposures in pulmonary lesions. *Nat. Med.* **26**, 529–534 (2020).
52. Chen, X. et al. Dynamic PET reveals compartmentalized brain and lung tissue antibiotic exposures of tuberculosis drugs. *Nat. Commun.* **15**, 6657 (2024).
53. Mota, F. et al. Dynamic (18)F-Pretomanid PET imaging in animal models of TB meningitis and human studies. *Nat. Commun.* **13**, 7974 (2022).
54. Ordóñez, A. A. et al. Molecular imaging of bacterial infections: Overcoming the barriers to clinical translation. *Sci Transl Med* **11**, (2019).
55. Ordóñez, A. A. et al. Visualizing the dynamics of tuberculosis pathology using molecular imaging. *J Clin Invest* **131**, (2021).
56. Bentley, J. K. et al. Rhinovirus colocalizes with CD68- and CD11b-positive macrophages following experimental infection in humans. *J. Allergy Clin. Immunol.* **132**, 758–761 e753 (2013).
57. Hong, J.-H. et al. Distribution of CD68-positive and CD11b-positive cells in the TRAMP-C1 tumors after high-dose in vivo irradiation. *Cancer Res.* **68**, 5335–5335 (2008).
58. Betjes, M. G. H., Haks, M. C., Tuk, C. W. & Beelen, R. H. J. Monoclonal-Antibody Ebm11 (Anti-Cd68) Discriminates between Dendritic Cells and Macrophages after Short-Term Culture. *Immunobiology* **183**, 79–87 (1991).
59. Lounis, N., Vranckx, L., Gevers, T., Kaniga, K. & Andries, K. In vitro culture conditions affecting minimal inhibitory concentration of bedaquiline against *M. tuberculosis*. *Med Mal. Infect.* **46**, 220–225 (2016).
60. Fortt, R., Smith, G., Awais, R. O., Luthra, S. K. & Aboagye, E. O. Automated GMP synthesis of [(18)F]ICMT-11 for in vivo imaging of caspase-3 activity. *Nucl. Med Biol.* **39**, 1000–1005 (2012).
61. Chen, R. et al. Tumor-to-blood ratio for assessment of fibroblast activation protein receptor density in pancreatic cancer using [68Ga] Ga-FAPI-04. *Eur. J. Nucl. Med. Mol. Imaging* **50**, 929–936 (2023).
62. Glatting, F. M. et al. Subclass analysis of malignant, inflammatory and degenerative pathologies based on multiple timepoint FAPI-PET acquisitions using FAPI-02, FAPI-46 and FAPI-74. *Cancers* **14**, 5301 (2022).
63. Scott, S. C. et al. Validation of a robust and rapid liquid chromatography tandem mass spectrometric method for the quantitative analysis of navitoclax. *Biomed. Chromatogr.* **36**, e5289 (2022).
64. Ruiz-Bedoya, C. A. et al. High-dose rifampin improves bactericidal activity without increased intracerebral inflammation in animal models of tuberculous meningitis. *J. Clin. Invest.* **132**, e155851 (2022).
65. Lin, S. F., Lin, J. D., Hsueh, C., Chou, T. C. & Wong, R. J. A cyclin-dependent kinase inhibitor, dinaciclib in preclinical treatment models of thyroid cancer. *Plos One* **12**, e0172315 (2017).

## Acknowledgements

We thank the Johns Hopkins University PET Center for assistance with <sup>18</sup>F-FAPI-74 synthesis. This work was funded by the National Institutes of Health [R01-AI153349, R01-AI145435-A1, R56-AI179012-A1, R01-AI190038, and S10-OD030381-A1].

## Author contributions

M.S. and S.K.J. conceptualized and designed the studies. <sup>18</sup>F-ICMT-11 precursor was developed and provided by E.O.A. M.O.S. and L.S.C. developed and performed the radiotracer syntheses for <sup>18</sup>F-ICMT-11 and <sup>18</sup>F-FAPI-74. M.S., A.K.S., Y.M.-L., and A.A.O. performed mouse studies. M.S. and N.N.L.D. performed the western blots. O.J.N.-M. performed the PET/CT imaging and analyses. M.S. analyzed the data in the manuscript. A.V.-R., X.C., C.E.R.-G., and F.R.-D. performed flow cytometry. S.K.J. provided funding and supervised the project. M.S. and S.K.J. wrote the manuscript. All the authors reviewed and edited the manuscript.

## Competing interests

The authors declare no competing interests.

## Additional information

**Supplementary information** The online version contains supplementary material available at <https://doi.org/10.1038/s41467-025-58190-x>.

**Correspondence** and requests for materials should be addressed to Sanjay K. Jain.

**Peer review information** *Nature Communications* thanks Reinout van Crevel and the other, anonymous, reviewer(s) for their contribution to the peer review of this work. A peer review file is available.

**Reprints and permissions information** is available at <http://www.nature.com/reprints>

**Publisher's note** Springer Nature remains neutral with regard to jurisdictional claims in published maps and institutional affiliations.

**Open Access** This article is licensed under a Creative Commons Attribution-NonCommercial-NoDerivatives 4.0 International License, which permits any non-commercial use, sharing, distribution and reproduction in any medium or format, as long as you give appropriate credit to the original author(s) and the source, provide a link to the Creative Commons licence, and indicate if you modified the licensed material. You do not have permission under this licence to share adapted material derived from this article or parts of it. The images or other third party material in this article are included in the article's Creative Commons licence, unless indicated otherwise in a credit line to the material. If material is not included in the article's Creative Commons licence and your intended use is not permitted by statutory regulation or exceeds the permitted use, you will need to obtain permission directly from the copyright holder. To view a copy of this licence, visit <http://creativecommons.org/licenses/by-nc-nd/4.0/>.

© The Author(s) 2025